Current Applied Physics 15 (2015) 78–83

Contents lists available at ScienceDirect

Current Applied Physics

journal homepage: www.elsevier.com/locate/cap

TCAD simulation of tunneling leakage current in CaF_2/Si(111) MIS structures

Yu.Yu. Illarionov [a, b, *], M.I. Vexler [a], M. Karner [c], S.E. Tyaginov [a, b], J. Cervenka [b], T. Grasser [b]

[a] Ioffe Physical-Technical Institute, 26 Polytechnicheskaya Str., 194021 St.-Petersburg, Russia
[b] TU Vienna, Institute for Microelectronics, 27-29 Gusshausstr., 1040 Vienna, Austria
[c] Global TCAD Solutions GmbH, Landhausgasse 4/1a, 1010 Vienna, Austria

ARTICLE INFO

Article history:
Received 26 July 2014
Received in revised form
2 October 2014
Accepted 26 October 2014
Available online 30 October 2014

Keywords:
Calcium fluoride
MIS structure
Tunneling current
Minimos-NT
Effective thickness

ABSTRACT

We introduce a simulation technique suitable to model the tunneling leakage current in the metal(-polySi)/CaF_2/Si(111) MIS structures using TCAD simulators Minimos-NT and ViennaSHE. The simulations are performed using the real physical parameters of the CaF_2/Si tunnel barrier. The results obtained for the case of near-equilibrium carrier transport are in a good agreement with experimental data and also with the simulation results yielded by our reference physical model. The obtained non-equilibrium hot-electron tunnel leakages in the hypothetical transistors with CaF_2 as a gate dielectric are comparable to those in the structures with silicon dioxide. Being an important step forward for the device application of calcium fluorite, this work opens the possibility of simulating the characteristics of different silicon-based systems with crystalline insulators.

1. Introduction

Calcium fluoride (CaF_2) is a crystalline insulator with high dielectric constant and wide bandgap (Table 1). Due to the proximity of its lattice constant to that of Silicon, it can be epitaxially grown on Si(111) substrates, potentially enabling creation of multilayer device systems. Nevertheless, for a long time CaF_2 has been considered an exotic material, not to mention that decades of work were necessary to overcome growth problems related to the formation of pinholes and other issues. Fortunately considerable progress in understanding the growth processes and electrophysical properties of fluorite has been made within the last years [1,2], which today is close to reaching device-relevant quality. Thus, thin fluorite films are now considered for practical applications as the insulating barrier layers in silicon solid state devices such as Resonant-Tunneling Diodes (RTDs) and super-lattices employing Si [3], CdF_2 [4] or Fe_3Si [5] quantum wells. At the same time, the idea of employing thin fluorite layers as a gate dielectric in the Field-Effect Transistors (FETs) [6] is now being reconsidered.

Along with a necessity for further film growth optimization, there appears a demand for more robust simulations of the main characteristics of fluorite-based structures. Recently we have demonstrated the possibility to reproduce the current–voltage (IV-) characteristics of CaF_2-based tunnel Metal-Insulator-Semiconductor (MIS) capacitors without fitting any parameters [7,8]. The next task in this direction is to use this model in TCAD simulators to predict the behavior of devices with thin calcium fluoride films in different operation modes. In this work we simulate the tunnel currents through thin fluorite layers in MIS systems using the TCAD tools Minimos-NT [9] and ViennaSHE [10], which so far has been applied only for the devices with SiO_2 and high-k oxides. Beyond the simulation of the usual quasi-equilibrium IV-characteristics we will perform an analysis of the effect of non-equilibrium hot carriers on tunnel charge transport in the mentioned devices.

The central place in the paper will be devoted to the question on how to adapt these TCAD simulators to the case of fluorite. This presumes the physics-based optimization of the tunneling probability formulas and consideration of both electron and hole current components. The theoretical results obtained in this study will be compared to experimental results for Au/CaF_2/pSi(111) structures obtained previously [11]. The CaF_2 film thickness under consideration will range from about 1.0 to 2.5 nm; it is dictated by a practical relevance, because the ultrathin (<2 nm) fluorite layers are of special interest in the context of applications in RTDs, FETs and most other devices.

* Corresponding author. TU Vienna, Institute for Microelectronics, 27-29 Gusshausstr., 1040 Vienna, Austria.
E-mail address: illarionov@iue.tuwien.ac.at (Yu.Yu. Illarionov).

http://dx.doi.org/10.1016/j.cap.2014.10.015
1567-1739/

2. Tunneling probability for the CaF_2/Si system

As of today, the values of Si/CaF_2 barrier parameters are rather well known [12] (Table 1). Particularly, the effective carrier mass for both allowed bands of the fluoride is $m_e = m_h = 1.0\ m_0$ within a parabolic law (adopted further) or $m_F = 1.2\ m_0$ with a Franz law.

The barrier height at the Au/CaF_2 interface $\chi_m = 2.63$ eV. This value relies on our experience in fabrication and characterization of MIS structures with calcium fluoride. The band diagrams calculated for Au/CaF_2/p-Si structure using Minimos-NT [9] are given in Fig. 1. Taking into account the barrier asymmetry and the wide band gap of fluoride one assumes that in all cases tunneling will take place through evanescent states derived from the CaF_2 conduction band (i.e. through the "top" barrier).

In the WKB approximation, the tunneling probability is.

$$T(E,k_\perp^2) = \exp\left[-2\hbar^{-1}\int\sqrt{2m_e\left(E_{cl}(z) - E + \hbar^2k_\perp^2/2m_e\right)}\mathrm{d}z\right] \quad (1)$$

where E is carrier energy (with zero at E_{c0}, s. right Fig. 1), $k_\perp$ – transverse momentum component and E_{cl} – coordinate-dependent energy of CaF_2 conduction band edge. Eq. (1) is also used for the case of carrier transport between the metal and Silicon valence band.

Often, attempts are being made toward converting this expression into the form of $T^*(E, E_\perp)$ where $E_\perp$ is the transverse energy of the tunneling particle. T^* is found by averaging Eq. (1) over all the electron states in the k-space (specified by a parameter "α") with the given $\{E, E_\perp\}$ pair:

$$T^*(E,E_\perp) = \left\langle T\left(E,k_\perp^2(E,E_\perp,\alpha)\right)\right\rangle_\alpha. \quad (2)$$

In the case of tunneling through an amorphous dielectric layer (e.g. SiO_2), or carrier transport from the valence band, or Si (100) substrate, Eq. (2) simplifies to

$$T^* = T(E, 2m_\perp E_\perp \hbar^{-2}), \quad (3)$$

where $m_\perp$ is the electron mass in Si in the surface plane. However, this does not work for the conduction band transport through a crystalline CaF_2 film on Si(111) substrate because of the large transverse momentum $k_\perp$ ("$k_\perp$-effect") for the tunneling electrons, especially near the very minimum k_0 of the indirect band ($k_{0\perp} = (2/3)^{1/2}\cdot k_0$) [7].

An optimized model can be introduced by assuming that the presence of $k_\perp$, which is different for different states with the given values of E and $E_\perp$, is equivalent to a shift ΔE of the tunneling electron energy. The largest shift $\Delta E_0 = \hbar^2k_{0\perp}^2/2m_0 = 2.44$ eV is obtained for $E = E_\perp = 0$, and for higher energies the situation approaches the direct band gap case, i.e. $\Delta E \to 0$. Finally, the tunneling probability for the CaF_2/Si(111) system is written as.

$$T^*(E,E_\perp) = \exp\left[-2\hbar^{-1}\int\sqrt{2m_e(E_{cl}(z) - E + m_\perp m_e^{-1}E_\perp + m_0m_e^{-1}\Delta E(E))}\mathrm{d}z\right] \quad (4)$$

where the dependence $\Delta E(E)$ is

$$\Delta E = \Delta E_0 \exp(-E/E_s). \quad (5)$$

The optimum value for the parameter E_s can be found by screening the simulation results for the electron current versus the insulator voltage $j(U)$ for the case of gate injection (left Fig. 1)

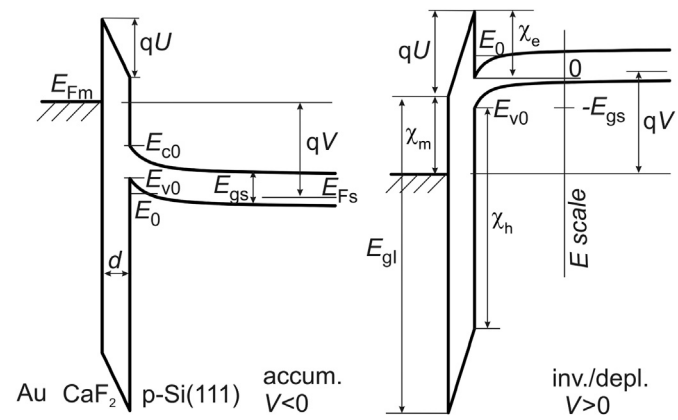

Fig. 1. Band diagrams of a MIS structure with a tunnel-thin fluorite film (in scale).

Table 1
Simulation parameters. V_{FB} is the flat-band voltage; ε_I, ε_S are permittivities; ζ_I – electron affinity; ΔE_0, E_s – factors in the formula for effective energy reduction of a tunneling electron (s. text), N_{it} is interface trap density. The barrier heights are labeled in Fig. 1.

CaF_2 parameters		Studied Au/CaF_2/Si system parameters		Essential Si wafer parameters	
ε_I	8.43	χ_e, eV	2.38	ε_S	11.9
E_{gI}, eV	12.1	χ_h, eV	8.6	E_{gs}, eV	1.12
m_e/m_0	1.0	N_{it}, cm^{-2}	10^{12}	orient.	(111)
m_F/m_0	1.2	χ_m, eV	2.63	ΔE_0, eV	2.44
ζ_I, eV	1.67	V_{FB}, V	−0.7	E_s, eV	1.0

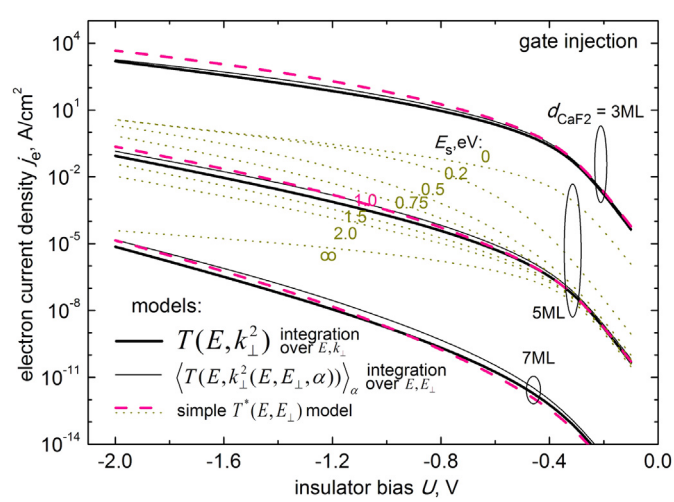

Fig. 2. Determination of the parameter E_s of the simple model for the electron tunneling probability by comparison with the results for the current yielded by the more precise models.

obtained after Eqs. (4) and (5) to the reference calculated with Eq. (2). The standard expression for this current is [7]: $|j_e| = 4\pi q \nu_\perp m_\perp h^{-3} \cdot \int [f_m(E) \int T^*(E,E_\perp) dE_\perp] dE$ where f_m is the metal Fermi function and $\nu_\perp = 6$ is the valley degeneracy. Taking U (not the gate bias V) as an argument (Fig. 2) this calculation relies neither on a specific model for the voltage partitioning nor on the Si dopant type. As can be seen from Fig. 2, the best fit is obtained by setting E_s to 1.0 eV. In that figure the curves generated using both Eq. (1) and (2) (the latter requires integration over E and $k_\perp$ [7,8]) are shown as a reference. Note that the fluoride thicknesses in Fig. 2 are given in monolayers (ML) which is natural for a crystalline dielectric. For CaF_2 there is 1 ML = 0.315 nm.

3. Tunneling current model: implementation and results

In this work Minimos-NT device simulator [9] is used for the simulations of near-equilibrium carrier transport and the deterministic Boltzmann transport equation solver ViennaSHE [10] is employed when dealing with hot electrons. Earlier, the simulator Minimos-NT has been successfully applied for simulations of a wide spectrum of different effects encountered in production quality devices, such as time-dependent reliability of nanoscale MOSFETs [13]. The simulator ViennaSHE uses the Spherical Harmonics Expansion (SHE) approach for the solution of the Boltzmann transport equation [14] and has already been successfully applied for the treatment of hot-carrier degradation (HCD) effects in the transistors of traditional architecture with SiON films [15,16]. Keeping the application perspectives of calcium fluoride in mind, it seems to be reasonable to employ these simulation tools also for the CaF_2-based MIS devices.

The current flowing through the MIS structure with CaF_2 is obtained as a sum of the electron and hole components. Note that it would be more correct to formulate the problem in terms of the currents of exchange between the metal and the Si conduction band, or metal and Si valence band, as transport of a hole can be interpreted as transport of an electron in the opposite direction, and vice versa:

$$j = j_e + j_h \tag{6}$$

It is commonly known that the states of carriers are quantized near the insulator/Si interface, so that discrete levels are formed (the level E_0 is shown in the diagrams of Fig. 1). For a physically rigorous approach, this effect has to be considered when modeling the currents. Also, in our own reference physical simulator (RPS) [7,8] one of the components (j_h in the left Fig. 1 or j_e in the right) contains a contribution from the discrete-levels plus the continuum current. The RPS program will be used below for some comparative calculations.

However, in most TCAD simulators such as Minimos-NT and ViennaSHE, the discrete states are only approximately considered by the introduction of quantum corrections to the density of states. Due to these corrections, the surface potential φ_s (for the given bias V) approaches its exact value; otherwise it would have been much lower. This correction function $\xi(E)$ is included also into the formulas for the current:

$$j_{e|h} = \frac{4\pi q \nu_\perp m_\perp}{h^3} \int_{E_{\min}}^{E_{\max}} \xi(E)(f_s(E) - f_m(E)) \int_0^{E_{\perp\max}(E)} T^*(E, E_\perp) dE_\perp dE \tag{7}$$

Here f_m and f_s are the carrier distribution functions for metal and Si, in the quasi-equilibrium case they are Fermi functions. The integration limits in (7) are $E_{\min} = -\infty$, $E_{\max} = -E_{gs}$, $E_{\perp\max} = -E_{gs} - E$ for the current from the valence band and $E_{\min} = 0$, $E_{\max} = +\infty$, $E_{\perp\max} = E$ for the current from the conduction band. The correction function $\xi(E)$ for the electron quantum well (right Fig. 1), approaches 0 if $E \to 0$ and is equal to 1 if $E \geq q\varphi_s$ or $E < -E_{gs}$. The trends for the hole quantum well are evident.

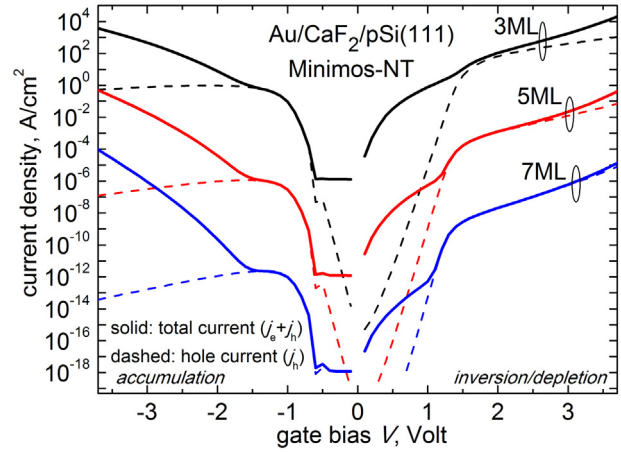

Fig. 3. IV-characteristics of Au/CaF_2/p-Si(111) structures with fluorite simulated using Minimos-NT.

The IV-characteristics simulated with the simplified model implemented in Minimos-NT for Au/CaF_2/p-Si(111) structures with three different insulator thicknesses are summarized in Fig. 3. These curves were obtained within a quasi-equilibrium approach inside the semiconductor for all bias conditions. They have all typical features known from the theory of tunnel MIS structures. Namely, there is an almost exponential increase of the current in the range of rather high voltages at any polarity. Furthermore, the total current $j = j_e + j_h$ (solid lines) depends very strongly on the fluorite thickness. Just left from the zero bias, there is a plateau because this range corresponds to the depletion of the semiconductor where the insulator voltage U does not follow the changes of the terminal bias V (the flat-band bias is $V_{FB} \sim -0.7$ V).

The dashed lines represent the valence band component j_h alone. In MIS studies it is often assumed that the electron component j_e is dominant while the hole part is neglected. The results shown in Fig. 3 unequivocally demonstrate the importance of the hole current in the CaF_2/Si(111) system. The energy of electrons which tunnel between the metal and the near-minima states of the conduction band of silicon is effectively reduced by the value of $\Delta E(E) > E_g$. As a consequence, the barrier for such electrons becomes higher than for the valence-band transport. With an increase in energy E, this effect gradually vanishes due to the exponent, cf. Eq. (6). All this means that one needs to deal with a complicated interplay between the two components.

Indeed, when a rather small accumulating bias is applied to the electrode (a little bit left from $V = V_{FB}$ in Fig. 3) the total current is mainly determined by j_h which is because the electron current j_e is blocked while E_{Fm} lies below E_{c0}. At higher negative bias j_h starts to decrease versus $|V|$ because the valence band tunneling occurs through the strengthening top barrier but the total current strongly increases due to a contribution of the electron component j_e. This component rapidly increases with increasing U and because the energies E of the involved electrons depart from E_{c0}, which reduces the ΔE-effect on the tunneling probability. In the inversion-depletion mode ($V > 0$) the hole current is blocked at low voltages, while E_{v0} is below E_{Fm}, while at higher positive voltages j_h comes into play and both components become comparable. The

Minimos-NT simulations predict that there is some range (near $V = 1.5$ V) where j_h is even dominant. At higher positive biases $j_e > j_h$, but the difference is not large enough for j_h to become negligible.

The results provided in Fig. 3 represent the first successful attempt to capture the essence of a carrier transport in MIS structures with fluorite films using the TCAD simulator. As we have just seen, an analysis of the underlying physics, e.g. of the interrelation between both tunneling current components, became possible. Evidently, a behavior of the total current j is strongly affected by an impact of the band structure on the electron current component. If the $k_\perp$-effect (ΔE-shift) had been neglected, all the values of the current would have been considerably higher. An important application of Minimos-NT is also clear: it potentially enables detailed consideration of a real device design. This is not critical while only the simplest structures are dealt with but will become necessary by even minimal complications of the configuration.

4. Comparison to other simulations and to experiment

In Fig. 4 the results for the structure with $d = 5$ ML simulated with Minimos-NT are compared to those obtained using our RPS assuming the accurate (with T^* after Eq. (2) for j_e) and simplified models, cf. Eq. (4). One can see that agreement is rather good. However, a slight difference between the obtained current values is still present which is due to the different models employed. In particular, for the Minimos-NT simulations the typical insulator bias U is a bit higher than in the RPS (see the inset). Furthermore, the expressions for the tunneling current (both j_e and j_h) are quite different: while Minimos-NT uses a continuum Eq. (7), our RPS separately treats also the discrete levels in the near-surface quantum well. In such a case a slight deviation between the results of the two simulators appears to be reasonable. Furthermore, the RPS also cannot be considered as perfect "calibration" tool. It is only important that there is no substantial qualitative and quantitative contradiction between the results of two different approaches. From Fig. 4 one concludes that the magnitude of the typical current difference between Minimos-NT and the RPS is of the same order as the discrepancy between the results of the accurate and simplified versions of the RPS itself.

Noteworthy, due to slightly larger insulator voltages U within Minimos-NT, the hole current j_h appears stronger at lower terminal

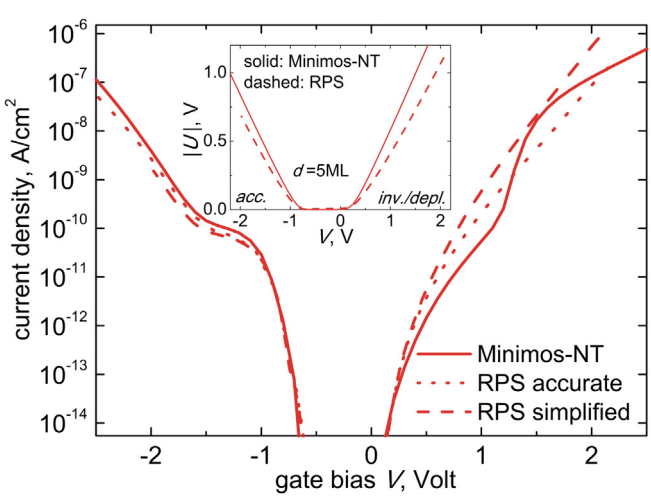

Fig. 4. IV-characteristics of the Au/CaF_2[5 ML]/p-Si(111) structure simulated with Minimos-NT and with the reference physical simulator (RPS) program assuming accurate or simplified tunnel probability models.

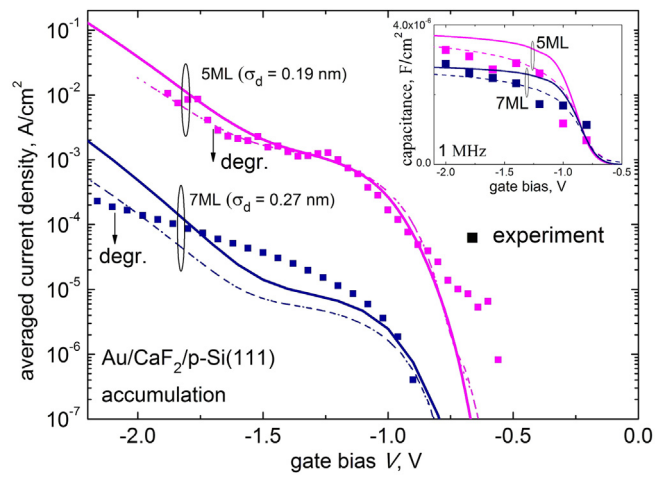

Fig. 5. IV-characteristics simulated using Minimos-NT under the assumption of thickness fluctuations compared to the experimental data and similar results obtained using the RPS program. Effective thickness model is used. Capacitance-voltage characteristics are given in the inset. Line styles correspond to those in Fig. 4.

voltages $V > 0$ than within the RPS, because the condition $E_{v0} > E_{Fm}$ is satisfied earlier. For this reason we see a hump in the $j(V)$ curve which is absent in the RPS case. In fact, the values of the CaF_2/Si barrier heights, although converged in the literature, nevertheless allow some variations. Again, it should be stressed that there is no serious disagreement between the models.

Next, we compare the theoretical results against experimental data measured on our MIS capacitor samples (Fig. 5). The curves (left from −0.7 V) correspond to accumulation mode which is more suitable for an analysis. (Under the reverse polarity, due to the minority carrier deficit in the two-electrode capacitors, the current relies rather on the thermal generation rate than on any insulator barrier properties; this complicates interpretation.). As a technical remark it has to be mentioned that such measurements slightly suffer from sample degradation, which results in a gradual decrease of the current especially in the high-bias range (arrows in Fig. 5). Qualitatively, the form of the characteristics agrees with expectations. However, for a purpose of quantitative comparison we should account for thickness fluctuation always occurring in practical samples. The fluctuations are usually measured by atomic-force microscope and obey the normal (Gaussian) distribution with a nominal value d_n and standard deviation σ_d (provided directly in Fig. 5).

Due to non-zero σ_d values for the measured films (Fig. 5), the results shown in Figs. 3 and 4 cannot be used for verification and should be re-generated. The fairest way would be to weight the current $j(d)$ with a Gaussian distribution. This is an elementary action but, to save computational resources, it is more convenient to employ an effective uniform thickness d_{eff}. The latter is introduced as $d_{eff} = d_n - \eta\sigma_d^2$, like it was earlier performed for SiO_2. This approach is based on the assumption $j(d) \sim \exp(-2\kappa d)$ $[\kappa = (2m_e\chi)^{1/2}\hbar^{-1}]$ for the local current density, with the "effective" barrier height $\chi \sim 3$–3.5 eV; such a density is then Gaussian-weighted. When d_n and σ_d are expressed in angstroms (Å), the value of η for CaF_2 can be estimated as 1.0.

The IV-characteristics simulated with the properly asserted fluoride thicknesses d_{eff} are included into Fig. 5. The simulations were performed using Minimos-NT and supported also by the RPS tool; the latter gives nearly the same curve for both the accurate and the simplified variant. In general, for each of the two nominal fluoride thicknesses, an agreement can be estimated as satisfactory, especially for the 5 ML sample. The most obvious discrepancy,

occurring also for the RPS, is in the slope of the characteristic for $d_n = 7$ ML, although even in that case the simulated current values are close to the measured data. This discrepancy arises from the use of d_{eff} and has been seen previously in similar studies of SiO_2 structures, if σ_d is relatively large. We have checked (not shown) that a Gaussian integration applied to the present simulation of Au/CaF_2/p-Si(111) structures yields better agreement for $d_n = 7$ ML. Furthermore, certain undervaluation of the currents at highest $|V|$ in Fig. 5 might be related to a degradation trend mentioned above. The inset to Fig. 5 shows the capacitance–voltage curves for the same samples (the range of accumulating bias). Otherwise than on the current, $k_\perp$ conservation has no impact on the capacitance; it was calculated like for the structures with SiO_2.

The progress in this work consisted in implementation of the appropriate tunneling model for the CaF_2/Si(111) case, where the old relatively simple approaches like the known Tsu-Esaki or the Fowler-Nordheim models would completely fail because of ignoring the $k_\perp$-effect (Section 2). Such kind simple approaches have been long ago implemented into Minimos-NT and many other simulators, enabling quite successful calculation of currents in MIS structures with amorphous oxides. A comparison of the predicted (using RPS) tunneling currents through CaF_2 and SiO_2, HfO_2, La_2O_3 was presented in our earlier work [17].

5. Simulation of the hot-electron induced effects

Hot-electron induced effects are rather important in the context of the device reliability. They have been investigated earlier in detail for devices with SiO_2 and SiON films [15,16,18]. However their consideration requires application of TCAD device simulators and is impossible with our RPS program. For this reason no attempts to incorporate the hot electron impact on devices with CaF_2 have been made so far. Thus, in this work the first attempt to address this issue with respect to the fluorite-based structures will be undertaken.

In the equilibrium case the electron distribution in Si is described by the standard Fermi function which has to be substituted into Eq. (7) instead of f_s. However, in the case of channel hot carriers one has to use a non-equilibrium distribution function.

$$f_s(E) = dn(E)/dE \cdot \rho_{3D}^{-1}(E) \cdot \xi^{-1}(E) \tag{8}$$

where ρ_{3D} is the usual density of states which is known for the Silicon band structure and behaves as ~ $E^{1/2}$ near the conduction band minimum. The energy distribution of electrons dn/dE (cm^{-3} eV^{-1}) is taken at the Si/CaF_2 interface. Near the equilibrium state Eq. (8) transforms into the standard Fermi function. Note that the term "distribution function" ("DF") is often used with respect to both dn/dE and f_s. This should not, however, cause a confusion as the units are evidently different, i.e. cm^{-3} eV^{-1} and dimensionless, respectively.

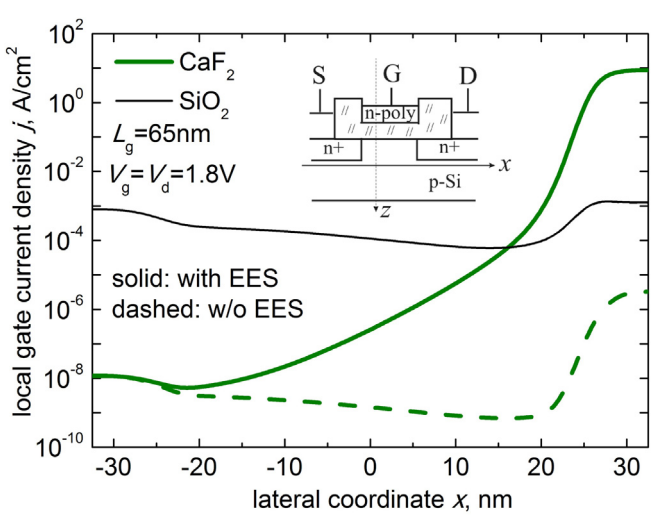

Fig. 6. Comparison of the tunnel leakages versus coordinate along the channel simulated for the MISFETs with CaF_2 and with SiO_2.

The physical situation with the hot electrons in a MIS structure can be illustrated for example by monitoring the heating along a MISFET channel, after which the electron leakage into the gate starts to dramatically increase. The magnitude of this leakage is considerably stronger than it would be without the impact of heating. This leads to hot-carrier degradation of the device, which is known to be one of the most important reliability concerns [15].

We next try to capture the essence of HCD for MISFETs with fluorite as a gate insulator. This is done with using ViennaSHE which has successfully been applied for production quality MOSFETs. The devices similar to *imec* design with a gate length $L_g = 65$ nm and CaF_2 thickness $d = 2.5$ nm corresponding to an effective oxide thickness $EOT = d \times \varepsilon_{\mathrm{ox}}/\varepsilon_I = 1.2$ nm are examined (see the configuration in Fig. 6, inset). The CaF_2/Si(111) surface state density N_{it} was set to 10^{12} cm^{-2}. The key feature of the simulations is the consideration of electron–electron scattering (EES) effects while calculating the non-equilibrium DFs using the deterministic simulator ViennaSHE [10]. This is of particular importance for ultra-scaled MISFETs and especially in the context of hot-carrier degradation which is very sensitive to high-energy tails of the DF [16,19].

In Fig. 6 the non-equilibrium leakage currents simulated for the devices with CaF_2 for $V_g = V_d = 1.8$ V are compared to those a similar device with SiO_2 (also $d = 2.5$ nm). One can see that near the source and in the center of the device the gate leakage is substantially lower in the CaF_2 based MISFET as compared to that simulated for the device with SiO_2. Near the drain, however, the gate current through the CaF_2 film appears to be higher. Such a trend is explained as a trade-off of two competing factors. On the one hand, the tunnel probability (calculated with a fixed carrier DF) is substantially suppressed in the CaF_2 film due to the higher dielectric permittivity ε_I, larger electron effective mass in CaF_2 (1.0 m_0 compared to 0.42 m_0 in SiO_2) and also due to the transversal shift $k_{0\perp}$. On the other hand, a higher ε_I value for CaF_2 leads to a higher electric field in the channel of the CaF_2-based transistor, so that the carriers are hotter, as compared to the device with SiO_2. The second tendency is further enforced by EES in the case of CaF_2 which dramatically increases the gate current near the drain. Note also that at relatively high V_d a substantial fraction of the electrons collected by the gate electrode is injected over the potential barrier. In the case of CaF_2, the height of the Si/dielectric barrier χ_e is lower than for SiO_2, which makes the effect even stronger.

6. Conclusion

In this work an attempt to apply the TCAD simulators Minimos-NT, ViennaSHE to model the carrier transport through thin calcium fluoride films has been performed. Real physical barrier parameters have been taken for this. The important point is that a numerical accuracy has been achieved and that the simulation results are in reasonable agreement with the experimental data for the case of equilibrium tunneling through the thin fluorite film. Also, the simulation technique has been tested for the case of hot-electron leakage from the MISFET channel. The presented modeling approach can be used in future to characterize different operational devices employing thin CaF_2 layers.

Acknowledgments

The authors acknowledge support by the Austrian Science Fund (FWF), grants P23598 and P26382, and the European Community FP7 projects No 261868 (MORDRED) and 619246 (ATHENIS 3D).

References

[1] M.I. Vexler, N.S. Sokolov, S.M. Suturin, A.G. Banshchikov, S.E. Tyaginov, T. Grasser, J. Appl. Phys. 105 (2009). Paper No. 083716.
[2] C. Deiter, M. Bierkandt, A. Klust, C. Kumpf, Y. Su, O. Bunk, R. Feidenhans'l, J. Wollschläger, Phys. Rev. B 82 (2010). Paper No. 085449.
[3] M. Watanabe, Y. Iketani, M. Asada, Jpn. J. Appl. Phys. 39 (2000) L964.
[4] M. Watanabe, T. Funayama, T. Teraji, N. Sakamaki, Jpn. J. Appl. Phys. 39 (2000) L716.
[5] K. Sadakuni-Makabe, M. Suzuno, K. Harada, H. Akinaga, T. Suemasu, Jpn. J. Appl. Phys. 49 (2010). Paper No. 060212.
[6] T.P. Smith, J.M. Phillips, W.M. Augustyniak, P.J. Stiles, Appl. Phys. Lett. 45 (1984) 907.
[7] M.I. Vexler, Yu.Yu. Illarionov, S.M. Suturin, V.V. Fedorov, N.S. Sokolov, Phys. Solid State 52 (2010) 2357.
[8] Yu.Yu. Illarionov, M.I. Vexler, S.M. Suturin, V.V. Fedorov, N.S. Sokolov, K. Tsutsui, K. Takahashi, Microelectron. Eng. 88 (2011) 1291.
[9] MINIMOS-NT User's Guide, Institute for Microelectronics, TU Wien, Austria.
[10] K. Rupp, T. Grasser, A. Jungel, IEDM Tech. Dig. (2011) 34.1.1–34.1.4.
[11] Yu.Yu. Illarionov, M.I. Vexler, V.V. Fedorov, S.M. Suturin, N.S. Sokolov, J. Appl. Phys. 115 (2014). Paper No. 223706.
[12] W. Hayes, Crystals with the Fluorite Structure: Electronic, Vibrational, and Defect Properties, Clarendon, Oxford, 1974.
[13] M. Bina, O. Triebl, B. Schwarz, M. Karner, B. Kaczer, T. Grasser, Proc. SISPAD (2012) 109–112.
[14] K. Rupp, T. Grasser, A. Jungel, Proc. SISPAD (2011) 151–154.
[15] M. Bina, K. Rupp, S. Tyaginov, O. Triebl, T. Grasser, IEDM Tech. Dig. (2012) 713–716.
[16] S. Tyaginov, M. Bina, J. Franco, D. Osintsev, O. Triebl, B. Kaczer, T. Grasser, Proc. IRPS (2014) 16.1–16.8.
[17] Yu.Yu. Illarionov, M.I. Vexler, S.M. Suturin, V.V. Fedorov, N.S. Sokolov, Tech. Phys. Lett. 36 (2010) 404.
[18] A. Gehring, T. Grasser, H. Kosina, S. Selberherr, J. Appl. Phys. 92 (2002) 6019.
[19] S. Rauch, F. Guarin, G. La Rosa, IEEE Trans. Device Material Reliab. 1 (2001) 113.